Thermal radiation and thickness fluctuations in freely suspended liquid films

Cite as: Phys. Fluids **18**, 085110 (2006); https://doi.org/10.1063/1.2337997
Submitted: 24 July 2005 • Accepted: 17 July 2006 • Published Online: 30 August 2006

Jie Zhang, X. L. Wu and Nasser Rashidnia

Thermal radiation and thickness fluctuations in freely suspended liquid films

Jie Zhang and X. L. Wu
Department of Physics, University of Pittsburgh, Pittsburgh, Pennsylvania 15260

Nasser Rashidnia
National Center for Microgravity Research at NASA Glenn Research Center, Cleveland, Ohio 44135

(Received 24 July 2005; accepted 17 July 2006; published online 30 August 2006)

Thermal convection in a vertically suspended soap film subjected to a vertical temperature gradient is marked by intense density fluctuations $\delta\rho_2$, uncommon to laboratory Rayleigh-Bénard convection (RBC). Such large fluctuations result from stratification in the film under the influence of gravity. Herein we present the first direct measurement of two-dimensional density fluctuations in a free-standing soap film using a single-point infrared detector. The radiation densitometer is nonintrusive and responds instantaneously to local density variations. Measurements of the power spectrum $\Gamma(f)$ of $\delta\rho_2$ are carried out using a variety of sample geometries of the aspect ratio of unity. In all cases, $\Gamma(f)$ scales with the frequency as $f^{-1.4\pm0.1}$ in the low frequency regime, which is in good agreement with the Bolgiano's theoretical prediction for a stably stratified fluid. Combining thermal imaging and particle tracking, we also show that it is feasible to measure the full-field density flux $\mathbf{j}(x,y)=\rho_2(x,y)\mathbf{v}(x,y)$ in the film. Despite that individual snapshots of $\mathbf{j}(x,y)$ appear random, the time-averaged flux forms a close loop similar to the large-scale circulation commonly seen in RBC, when a sufficiently large temperature gradient is present. © *2006 American Institute of Physics*.
[DOI: 10.1063/1.2337997]

I. INTRODUCTION

Studies of fluid flow and turbulence using freely suspended aqueous and liquid-crystal films have attracted much attention over the past decade.[1–9] This interest can be traced to the unique physical properties of these films being very thin such that the fluid motion can be treated as nearly two-dimensional (2D). It has been shown recently,[10] based on a general physical ground, that an aqueous film with a small amount of soluble surfactants obeys the 2D incompressible Navier-Stokes equation if the following three conditions are satisfied: (i) The in-plane velocity U varies on a scale L that is much larger than the film thickness h; (ii) U itself is much less than the elastic (or the Marangoni) wave velocity v_e, and (iii) the average film thickness h is uniform. The first condition is readily satisfied in most experiments since $h\sim 1$ μm and L is of the order of a few millimeters to several centimeters, making $h/L<10^{-3}$. On the other hand, the second condition is more demanding but can still be satisfied in many experiments since the elastic velocity of the film is $\sim$10 m/s (Refs. 1 and 10) and the typical turbulent velocity fluctuation v_{rms} is several tens of centimeters, making $v_{\mathrm{rms}}/v_e\sim 10^{-1}$ or less. The third condition ensures that the system can be treated as homogeneous and isotropic. In most experiments, condition (iii) is satisfied since the mean film thickness is almost uniform and the thickness fluctuations are small compared to the mean.[3] In the current study, we explored the situation in which the film thickness is not uniform but stratified strongly along the vertical direction. The violation of the third condition makes the film subject to intense density fluctuations and the incompressible condition is no longer strictly obeyed. This experiment demonstrates that freely suspended soap films have a great potential for exploring fluid physics in low spatial dimensions where new phenomena can be studied.[11–14]

A few years ago, we discovered that when a soap film is exposed to a large vertical temperature gradient, warm at the bottom and cold at the top, steady-state convection could be established.[15] The convection has the remarkable effect of prolonging the lifetime of such a film from a few seconds, if the temperature gradient were absent, to almost indefinitely. This is because the convective mass current continuously replenishes the fluid loss at the top of the film due to gravitational stratification, making the entire film more uniform. In the steady state, the thermal convection is vigorous, achieving a root-mean-square (rms) velocity v_{rms} of several centimeters per second in a film that measures only a few centimeters across. The phenomenon is in sharp contrast with earlier attempts using freely suspended liquid crystal films where convection velocity ~ 10 μm/s was observed.[16,17] The ability to induce strong convection in these freely suspended aqueous films makes them well suited for studying 2D convective turbulence, where there are many theoretical predictions[14,18–23] but with very few laboratory experiments.[24] This is especially the case for a stably stratified fluid.[25] However, since in the early experiment we were unable to measure either the temperature T or the film thickness h, the latter corresponding to the 2D mass density of the fluid $\rho_2(x,y)=\rho h(x,y)$, the behavior of these important dynamic variables remains largely unknown, where ρ is the mass density of water. This state of affairs provides a strong motivation for the current experiment.[26]

In this paper we report new studies of thermal turbulence

in freely suspended soap films. The experiment exploits the fact that long wavelength photons can readily escape from the interior of the film and can be detected by sensitive infrared (IR) detectors. These photons carry useful information about the local environment of the fluid, such as the temperature and the 2D density; both are important for quantitative understanding of turbulent convection when a temperature gradient is present. Unfortunately there is no off-the-shelf instrument that can be used to measure weak thermal radiation on time scales shorter than the fluctuation time of turbulence observed in the soap films. At the outset, it is not even clear if the idea is feasible, considering that the thermal mass of a soap film is so diminishingly small. One of the objectives of this paper is thus to demonstrate that weak thermal radiation from a local point in the soap film can be detected with the implementation of a remote IR sensing technique, which we termed the single-point radiation densitometer (SPRD). A full-field IR transmission imaging system is also implemented to visualize directly the entire film thickness profile$h(x,y)$.[27] The SPRD and the full-field IR imaging are complementary to each other in that the former is suitable for measuring fast ($\sim$1 ms) temporal variations of thermal radiation while the latter is slow (33 ms) but provides detailed spatial structures of the 2D mass distribution. The combination of the two methods allows us to draw the important conclusion that the measured spatial and temporal variations of the radiation signals are dominated by the fluctuations of the thermal emissivity of the film, which is related to the thickness or the 2D density of film. This is a subtle point and has not been properly dealt with in a recent experiment.[28]

The validity of our experimental techniques is tested by the investigation of temporal fluctuations of the 2D mass density in the film driven by a large temperature gradient. Interestingly, even with a moderate sized film (2×2 cm^2), the measured frequency power spectrum $\Gamma(f)$ of density fluctuations is in rather good agreement with the Bolgiano's theoretical prediction for a fluid that is stably stratified.[29] The steady-state density profile in the film is shown to be a function of the overall temperature gradient. An interesting density inversion, from the stably stratified to the unstably stratified profile, is observed when the temperature gradient is increased beyond a threshold. Remarkably, this coincides with the onset of a large-scale circulation (LSC). We also found, using simultaneously the full-field IR imaging and a particle image velocimetry, that the time averaged 2D mass flux forms a closed loop, spanning the entire convection cell even though individual flux fields appear to be spatiotemporally chaotic. The observation therefore demonstrates a subtle but important correlation between the velocity and the mass density in convective turbulence. These findings are new and their general implications for convection with a strong density profile, which is common in nature, remain to be explored.

This paper is organized as follows: In Sec. II, we introduced the experimental methods for creating 2D freely suspended films in a uniform temperature gradient. Section II B also contains a discussion about the driving mechanisms of thermal convection in the soap film. Section III is the main body of the paper, describing the measurements using SPRD and the 2D full-field imaging system. The frequency power spectra for various sample geometries are presented along with the steady-state 2D density profiles measured along the gravitational direction. Also presented in this section are the two-point statistics of density fluctuations and the mass flux measurements. Section IV provides a brief summary of our experiment and possible future experiments. Much of the experimental details, such as the calibration procedures and calculations, can be found in Ref. 30.

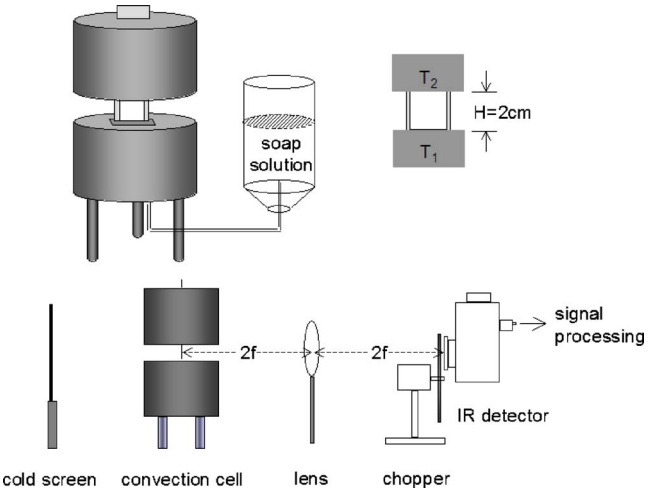

FIG. 1. Experimental setup. The experimental setup consists of a thermal convection cell, which is made of two large aluminum cylinders stacked on top of each other. Each cylinder measures 10 cm in diameter and 10 cm in height. The lower cylinder is heated by stick-on Minco heaters and the upper cylinder is cooled by four solid-state coolers. The separation of the two blocks can be adjusted so that films of different heights can be formed. Inside the lower heating block is a slim stainless steel vessel, which serves as a reservoir for the soap solution, and is connected to an external soap-solution bottle. The height of the soap solution inside the vessel is automatically adjusted. A thin stainless steel frame, 50 μm thick, is used to draw the film from the reservoir. For the current experiment, the height of the film was fixed at 2 cm. For the thermal radiation measurement, the imaging optics was set up such that a single point in the film was directly mapped onto the light detector using the 2f-2f geometry. In order to reduce noises, the incoming radiation signal was modulated by an optical chopper, amplified first by a preamplifier, and then sent to a lock-in amplifier. A HeNe laser was used to aid the alignment of the optics.

II. EXPERIMENTAL METHODS AND THE DRIVING MECHANISM

A. Thermal convection setup in freely suspended films

A schematic drawing of our experimental setup is shown in Fig. 1. Here two anodized aluminum blocks are used to stabilize the thermal gradient. The temperature T_1 (the lower block) and T_2 (the upper block) are controlled independently by two Tronac temperature controllers with a long-term stability of better than 10 mK. The two aluminum blocks are separated by an adjustable gap in which a freely suspended film is drawn from a reservoir imbedded in the lower block.

The main ingredients of the soap solution are 2% (by weight) Dawn liquid detergent and 98% of distilled water. To facilitate velocity measurements using laser Doppler velocimetry (LDV) and particle imaging velocimetry (PIV), small colloidal particles of 1 μm in diameter are seeded into the

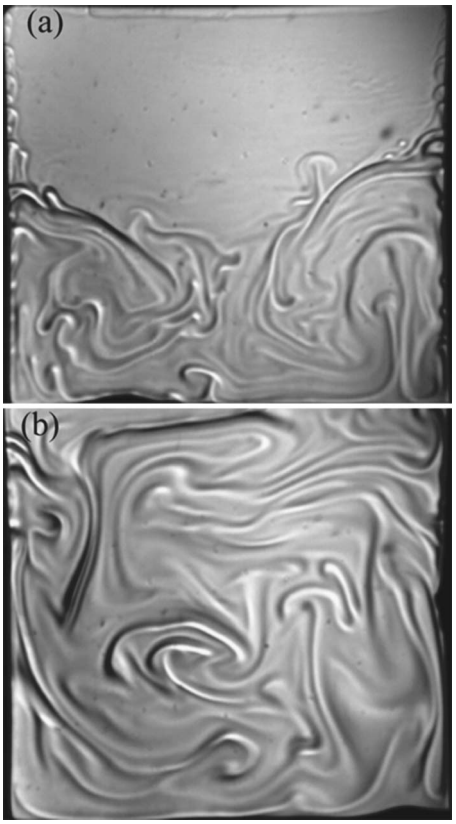

FIG. 2. Shadowgraphs of thermal convection patterns in soap films. The pictures were taken by a CCD camera with the shutter speed set at 1/1000 s. The height and the width of the film were, respectively, 2 by 2 cm. The temperature differences are $\Delta T=31\ ^\circ\mathrm{C}$ for (a) and $\Delta T=62\ ^\circ\mathrm{C}$ for (b). In both cases, thermal plumes of various sizes are clearly observed. However, for the low temperature gradient case (a), the plumes can only climb half way up the film, leaving the top half essentially quiescent. One can occasionally observe, as seen in (a) that a small plume ascends from the lower mixing region into the upper quiescent region. This type of plume is not as energetic as the ones directly ejected from the bottom of the cell. In the presence of the large temperature gradient (b), the plumes can readily reach to the top of the film, causing vigorous mixing throughout the entire cell.

fluid. The addition of these particles is shown to have little effect on fluid flows in the film. A thin stainless steel frame (50 μm thick) with a square hole ($2\times 2\ \mathrm{cm}^2$) cut in the center is used to initiate the film. When the hole is lowered into the soap reservoir and then raised slowly, a freely suspended film forms naturally and can last for a long time if the convection is active.

To appreciate what we attempted to study, it is useful to preview flows observed in the film. Figure 2 shows typical flow patterns when the temperature differences are, respectively, $\Delta T(=T_1-T_2)=31\ ^\circ\mathrm{C}$ (a) and $62\ ^\circ\mathrm{C}$ (b). The upper temperature T_2 is fixed at $14\ ^\circ\mathrm{C}$ for most measurements. A standard shadowgraph technique[31] is used and the pictures are taken with a normal CCD camera. As can be seen, for a relatively small temperature difference (a), the dominant flow structures are thermal plumes that are emitted constantly from the lower boundary, driving the fluid flow in the lower part of the film. The emission of thermal plumes from the upper boundary is rare. The asymmetric emission of plumes shows that our system is intrinsically different from the classical paradigm of Rayleigh-Bénard convection, where plume emission is more or less symmetric from the top and from the bottom.[32–35] This observation implies that when ΔT is not large, density stratification plays an important dynamic role in our system[15,23] and the potential energy overwhelms the kinetic energy of thermal plumes. This behavior is consistent with our earlier observation which shows that the onset of convection consists of nonlinear oscillatory waves instead of rolls because of the stable density gradient.[15] For large temperature differences ($\Delta T>48\pm 2\ ^\circ\mathrm{C}$), thermal plumes gain considerable more kinetic energy, allowing them to soar to the top of the film. In this so-called kinetic energy dominated regime (b), one observes that vigorous convection takes place throughout the entire film and a large-scale circulation (LSC) often forms and switches directions in a chaotic fashion. It appears that above a certain temperature gradient, thermal plumes have a tendency to aggregate near one of the side walls, forming so-called super plumes that rise rapidly along the vertical wall. These jet-like structures strongly bias the flow pattern in the cell. Despite the small system used, the typical flow velocity is rather high with $v_{\mathrm{rms}}\sim 3$–$5\ \mathrm{cm/s}$, which is much larger than the corresponding 3D systems.[36] The large velocity fluctuations in the film give the appearance of strong turbulence as depicted in the pictures.

B. Driving mechanism

When a soap film is exposed to a vertical temperature gradient, it is subjected to the buoyant force resulting from thermal expansion of water and from the inhomogeneities in the film thickness. The 2D density therefore should depend explicitly on these two contributions. Since $\rho_2(T,h)=\rho(T)h$, where both T and h are functions of the position (x,y) in the film and time t, it follows $d\rho_2=\rho_2(-\alpha dT+h^{-1}dh)$, where $\alpha=2.1\times 10^{-4}\ \mathrm{K}^{-1}$ is the thermal expansion coefficient of water. Moreover, a spatially nonuniform temperature distribution can induce a thermal capillary force on a film element, and it should be taken into account in the equation of motion of the film. The dynamics in a soap film are thus determined by the following set of coupled equations:

$$\frac{\partial \mathbf{v}}{dt}+\mathbf{v}\cdot\boldsymbol{\nabla}\mathbf{v}=\nu\nabla^2\mathbf{v}-\gamma\mathbf{v}+\frac{1}{\rho_2}\boldsymbol{\nabla}\Sigma-g\frac{d\rho_2}{\rho_2}\hat{y}, \tag{1}$$

$$\frac{\partial T}{\partial t}+\mathbf{v}\cdot\boldsymbol{\nabla}T=\kappa\nabla^2T-\frac{2\sigma(T^4-T_0^4)}{c\rho_2}-\gamma'(T-T_0), \tag{2}$$

$$\frac{\partial \rho_2}{\partial t}+\mathbf{v}\cdot\boldsymbol{\nabla}\rho_2=-K\nabla^4\rho_2-\bar{\rho}_2'v_y. \tag{3}$$

Here the gradient operator $\boldsymbol{\nabla}\left(\equiv\partial/\partial x\hat{x}+\partial/\partial x\hat{y}\right)$ is two-dimensional, ν is the film viscosity, γ is the air drag coefficient, Σ is the surface tension, g is the gravitational constant, κ is the thermal diffusivity of water, σ is the Stefan-Boltzmann constant, c is the specific heat of water, $T_0=(T_1+T_2)/2$ is the average temperature in the convection cell (assuming well mixed air), γ' is the conductive heat transfer coefficient to air, $K=\Sigma h^3/12\pi\eta$ is an effective diffusion coefficient for the 2D density,[15] and $\bar{\rho}_2'$ is the mean 2D density

gradient. Note that the pressure gradient term normally associated with a 3D fluid is here replaced in Eq. (1) by the surface-tension gradient term, and it is related to the temperature gradient by $\nabla\Sigma=(\partial\Sigma/\partial T)\nabla T$. Equation (2) is a convective diffusion equation for the temperature field, taking into account the heat loss due to thermal radiation and conduction. For heat conduction to air, we have assumed the simplest thermal coupling between the film and the air, known as the Newton's law of cooling. Though the value of γ' is not presently known, its overall effect is to fasten the cooling of the film.[37] The flow in a soap film is three-dimensionally incompressible but in general is two-dimensionally compressible. This is described by the last equation. Here the constant K plays the role of "diffusion" for the 2D density (or the thickness). The appearance of $\nabla^4\rho_2$, instead of the usual Laplacian, is connected with the fact that fluid flow inside the film is assumed to obey Darcy's law (velocity proportional to pressure gradient).[15] Consequently, density inhomogeneities relax very slowly for a thin film. The last term in Eq. (3) describes the coupling between the mean density gradient $\bar{\rho}_2'$ with the vertical velocity v_y and is the source for the intense density fluctuations. Equations (1)–(3) are general, expressing conservation of momentum, energy, and fluid mass, respectively. Since we do not attempt to solve this model, no Boussinesq approximation is made. Such approximation probably will not work too well in our experiment because of the large temperature and density fluctuations present. To fully specify the problem, the boundary conditions are needed, especially for the velocity field. The velocity field on the top and the side walls is zero (the nonslip condition) but the bottom boundary obeys a nonstress condition because of the film is in contact with the reservoir. The specific boundary conditions are significant for the onset behavior, but for strong turbulent convection they are expected to play a lesser role. This is consistent with the visual observation that the presence or the absence of the reservoir does not change turbulent convection patterns significantly in the film. Equations (1)–(3) show that the dynamics in the soap film is double diffusive, characterized by two scalar fields $T(x,y,t)$ and $\rho_2(x,y,t)$. However, as the following analyses indicate, hydrodynamic fluctuations in the interior of the film are essentially dominated by the thickness field and the temperature effect (or for that matter the surface tension gradient) is mostly confined to within a thin layer near the boundary. This behavior is somewhat similar to RBC, but for a different mechanism.

Inspection of Eq. (2) shows that the typical time scale τ and the length scale ξ associated with cooling of a patch of a film due to thermal radiation and heat conduction to air are given by $\tau^{-1}=8\sigma T_0^3/(c\rho_2)+\gamma'$ and $\xi^2=\kappa\tau=\kappa/[8\sigma T_0^3/(c\rho_2)+\gamma']$. Here we have ignored the convective term and used the approximation $T-T_0\ll T_0$ to linearize the radiation term. Since the value of γ' is not known, in the following analysis we will estimate τ and ξ based on thermal radiative loss alone. Using values from our experiment: $h\sim 2\ \mu$m, $T_0=320$ K, $c=4.2\times10^7$ erg g^{-1} K^{-1}, $\sigma=5.67\times10^{-5}$ erg s^{-1} cm^{-2} K^{-4}, and $\kappa=1.3\times10^{-3}$ cm^2 s^{-1}, we found $\tau\sim0.6$ s and $\xi\sim270\ \mu$m. Thus, a rising plume cools rather quickly by thermal radiation. If heat conduction to air is also taking into account, the cooling time τ will only be shorter. The smallness of the thermal coherent length ξ suggests that the mean temperature in the film plane relaxes rather quickly from the boundary with the result $T(y)\sim\sinh(y/\xi)$.[17] In the interior of the film $y\gg\xi$, away from the boundary, the temperature is essentially uniform. These calculations are not surprising, reflecting the fact that a micron thick film contains very little thermal energy and radiative cooling is sufficient to take out all thermal energy in a short time and over a small length scale. It has been suggested that this fast heat dissipation was largely responsible for the slow flow velocity observed in freely suspended liquid crystal films.[17]

As for most hydrodynamic problems, it is useful to write the equations of motion in a nondimensional form. This can be done by rescaling length by the height of the film H, the time by H^2/ν, the velocity by ν/H, the surface pressure Σ by the kinetic energy $\rho_2 v^2/2=\rho_2(\nu/H)^2/2$, the temperature fluctuations in the film $\delta T=T-T_f$ by the overall temperature gradient ΔT, and density fluctuations $\delta\rho_2$ by the overall density gradient $\Delta\rho_2$ in Eqs. (1)–(3), where T_f is the average film temperature profile. The resulting equations are simplified and given by

$$\frac{\partial\mathbf{v}}{dt}+\mathbf{v}\cdot\nabla\mathbf{v}=\nabla^2\mathbf{v}-\Gamma\mathbf{v}+\nabla\Sigma+\left(\frac{\mathrm{Ra}}{\mathrm{Pr}}T-\frac{\mathrm{Ra}'}{\mathrm{Pr}'}\rho_2\right)\hat{y}, \tag{4}$$

$$\frac{\partial T}{\partial t}+\mathbf{v}\cdot\nabla T=\frac{1}{\mathrm{Pr}}\nabla^2T-\Gamma'(T+T_{f0}), \tag{5}$$

$$\frac{\partial\rho_2}{\partial t}+\mathbf{v}\cdot\nabla\rho_2=-\frac{1}{\mathrm{Pr}'}\nabla^4\rho_2. \tag{6}$$

Here, the field variables are reduced quantities, i.e., $\mathbf{v}\equiv\mathbf{v}/(\nu/H)$, $T=\delta T/\Delta T$, $T_{f0}=(T_f-T_0)/\Delta T$, and $\rho_2=\delta\rho_2/\Delta\rho_2$. In the special case when the average film temperature is equilibrated with the surrounding air, Eq. (5) is simplified because $T_{f0}=0$. The above equations contain four control parameters corresponding to the Rayleigh number $\mathrm{Ra}=\alpha gH^3\delta T/(\nu\kappa)$ and the Prandtl number $\mathrm{Pr}=\nu/\kappa$ for the temperature field, and the Rayleigh number $\mathrm{Ra}'=gH^5\delta\rho_2/(\rho_2^0\nu K)$ and the Prandtl number $\mathrm{Pr}'=\nu H^2/K$ for the 2D density field, where $\delta\rho_2=\rho_0\delta h$, $\rho_0=\rho(T_f)$, and $\rho_2^0=\rho_0 h_0$ with T_f and h_0 being the average temperature and thickness. The other two dimensionless parameters, $\Gamma=H^2\gamma/\nu$ and $\Gamma'=H^2/(\nu\tau)$, characterize, respectively, the effect of air in velocity damping and heat leakage in the film. One can estimate the typical values of the control parameters based on our experimental observations ($\Delta T\approx50$ K, $h_0\approx3\ \mu$m, and $\Sigma\approx40$ erg/cm^2), yielding $\mathrm{Ra}\approx6.5\times10^6$, $\mathrm{Pr}\approx7.7$, $\mathrm{Ra}'\approx3.2\times10^{14}$, and $\mathrm{Pr}'\approx1.4\times10^7$. We note that in our system $\mathrm{Pr}'\gg\mathrm{Pr}$, indicating that the 2D density is a much more slowly evolving field than the temperature, and consequently it determines the long-time, nonlinear behavior of the system. Moreover, the contributions of the scalar field ρ_2 and T to the velocity equation (4) are functionally identical with coefficients Ra/Pr and $\mathrm{Ra}'/\mathrm{Pr}'$. However, since the ratio $\mathrm{Ra}'/\mathrm{Pr}'$ is about a factor of 10 greater than Ra/Pr, it indicates that the dominant driving force, at least in the in-

terior of the film, is the 2D density rather than temperature fluctuations. The viscous and thermal couplings of the film to air ($-\Gamma \mathbf{v}$ and $-\Gamma' T$) are significant so far as the total energy budget of the system is concerned. However, their influences on spatial/temporal fluctuations are subtle. In an earlier experiment, it was shown that weakening of the viscous coupling to air by enclosing the film in partial vacuum does not alter the velocity power spectrum of 2D grid turbulence even though the overall fluctuation is increased.[38] In the present case, however, it is unclear if the density power spectrum, which is to be reported below, is also unaffected by the thermal coupling term in Eq. (2) or (5).

A tentative physical picture of soap film convection therefore can be summarized as follows: the temperature gradient is mostly confined within a small region $\sim\xi$ near the cell boundary. Inside this boundary layer, the temperature gradient is very large and causes intermittent burst of thermal plumes. The detailed dynamics of plume emission is not known but it is likely the combination of buoyancy and the Marangoni effect. A simple back-of-the-envelop calculation shows, the emission velocity v_p of a plume of size $l_p \sim 0.2$ cm can be related to the surface tension gradient as $(d\Sigma/dT)\Delta T \xi^2 \sim \rho h l_p^2 v_p^2$. Taking $d\Sigma/dT \sim 0.04$ dyn cm^{-1} K^{-1}, $\Delta T = 10$ K, and $h \sim 2$ μm, we found $v_p \sim 6$ cm/s, which is of the order of magnitude consistent with the observed value $v_p = 3.5$ cm/s. The existence of a thermal boundary layer is not unique to a soap film. In highly turbulent 3D RBC, such a layer also exists and is stabilized by turbulence in the interior of the fluid.[33] Thus the physical mechanisms for boundary layer formation in 2D and 3D are entirely different.

Because the cooling is rapid, the rising plumes provide primarily the kinetic energy (not the thermal energy) to the interior of the film and cause turbulent mixing in the lower part of the film. Increasing the temperature gradient, the incipient plumes ascent with greater kinetic energy, the lower mixing zone expands. The physics in the interior of the soap film is therefore considerably different than in the boundary layer. Inside the film, fluid motion is strongly influenced by density stratification and the temperature field only plays a minor role. The fluctuations in temperature and in density are essentially decoupled because of the separation of time scales, i.e., temperature fluctuations relax much faster than the 2D density (or the film thickness). The net result is that soap-film dynamics in the interior of the film is essentially governed by Eqs. (1) and (3), which represent a stratified turbulence system similar to the ones treated by Bolgiano.[29] The lack of temperature sensitivity in the interior of the film can be demonstrated in our system simply by reversing the temperature gradient. In this case turbulence is completely suppressed suggesting fluid flows in the film are driven by density inhomogeneities rather than the surface tension gradient.

C. Thermal radiation from semitransparent films and its measurements

Reliable temperature and thickness measurements in a freely suspended liquid film are not trivial. This is in part due to the small thickness and in part due to the fluid motion in the film. Using the temperature measurement as an example, the small film thickness contributes to a small thermal mass, which can be easily perturbed by a conventional contact thermometer, making the measurement inaccurate. Likewise, wetting of the fluid on the temperature sensor could also significantly distort the planar geometry of the film, obstructing fluid flows. We note that a typical freely suspended film used in our experiment has thickness at least a factor of 10 smaller than the smallest thermistor (~ 100 μm in diameter) or thermocouple (~ 50 μm in diameter) commercially available. To study convection in the film, therefore, it is highly desirable if a noninvasive and fast-response probe is used.

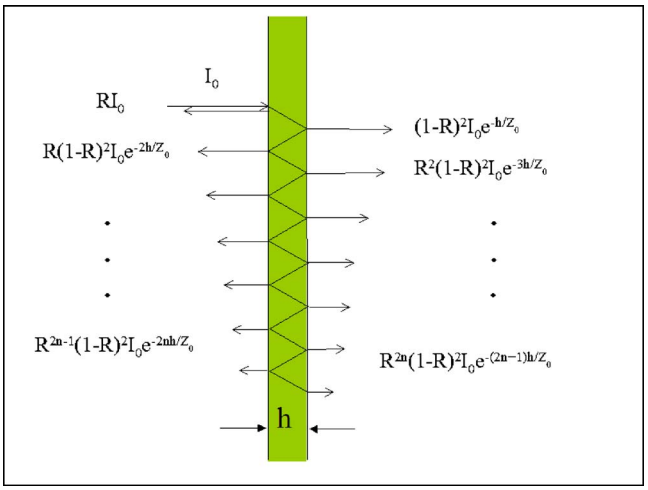

FIG. 3. A schematic diagram of multiple-beam reflection in a soap film. The input light I_0 is multiply reflected and attenuated due to IR light absorption. The film is assumed to have a uniform thickness h and a constant absorption length Z_0. The light reflectivity r, transmittance t, and emissivity s, are calculated based on this geometry. See text for details.

We have designed and tested an infrared (IR) radiometer, which allows us to measure rapid fluctuations of thermal radiations emitted from a single point in the film. Thermal radiation from an arbitrary object obeys the Stefan-Boltzmann equation $I = s\sigma T^4$ and the emission is peaked at $\lambda_{\max} = 0.0029/T$ (K m) for the given temperature T, where s is the thermal emissivity of the emitter, σ is the Stefan-Boltzmann constant, and I is the total radiation energy flux. For the typical temperature used in the experiment, ~ 60 °C, $\lambda_{\max} = 8.7$ μm. The thermal emissivity s is determined by the Kirchoff's law $s+r+t=1$, where r is the reflectivity of the surface and t is the transmittance. If the body is opaque with $t=0$, the surface reflectivity alone determines the thermal emissivity with $s+r=1$. In our thin liquid films with a finite thickness h, the transmittance t cannot be neglected. However, s can still be determined based on the generalized Fresnel's law of reflection, which takes into account the light absorption property of the material. Using the schematics in Fig. 3 and assuming a single absorption length $Z_0 = Z_0(\lambda)$, the reflectivity and the transmittance can be calculated with the results:

$$t = \frac{I_t}{I_0} = \frac{(1-R)^2 e^{-h/Z_0}}{1 - R^2 e^{-2h/Z_0}}, \tag{7}$$

$$r = \frac{I_r}{I_0} = R\frac{1 + (1-2R)e^{-2h/Z_0}}{1 - R^2 e^{-2h/Z_0}}, \tag{8}$$

$$s = 1 - r - t = 1 - \frac{(1-R)^2 e^{-h/Z_0} + R(1 + (1-2R)e^{-2h/Z_0})}{1 - R^2 e^{-2h/Z_0}}, \tag{9}$$

where R is the reflectivity at the water-air interface. The bulk water is an excellent radiator due to its low reflectance and high absorption in the near IR regime. For instance, at $\lambda \sim 2.98$ μm, the attenuation length Z_0 is only 0.9 μm; a film of a few microns in thickness is essentially opaque and all the exponential term in Eqs. (7)–(9) can be dropped and s is constant independent of h. Measurements show that the thermal emissivity of bulk water is quite high with $s = 1 - R \sim 98\%$, yielding $R \sim 2\%$ over the wavelength range $3 < \lambda < 14$ μm, which is relevant to the IR radiometer implemented in this experiment.[39] The small R allows the calculation of s for an aqueous film to be simplified. To the first order in R, we find

$$s \approx (1 - e^{-h/Z_0}) - R(1 - e^{-h/Z_0})^2. \tag{10}$$

The leading thickness dependence is thus given by

$$s \approx 1 - e^{-h/Z_0}, \tag{11}$$

if the contribution of R is neglected. The above derivation shows that thermal radiation can be used to measure separately the temperature (a radiation thermometer) and the film thickness (a radiation densitometer) depending on the detection wavelength λ. For those wavelengths for which water absorbed strongly ($Z_0 \ll h$), the thermal radiation is dominated by the temperature fluctuations since $s \sim 1$. In the opposite limit ($Z_0 \gg h$), the technique is sensitive to temporal fluctuations in the thermal emissivity, which can be directly related to variations in the film thickness since $s \sim h/Z_0$. In the thin-film limit, $h/Z_0 \to 0$, thermal radiation diminishes as expected.

To measure thermal radiation from the film we used a mercury-cadmium-tellurium (HgCdTe) detector purchased from EG&G. The detector was installed in a double-window Dewar and cooled down to the liquid nitrogen temperature of 77 K. A small spot in the center of the film, ~1 mm in diameter, was imaged onto the photodetector by a ZnSe lens (II-VI, Inc). The lens has a high numerical aperture (f-number=0.8 with FL=2.25 cm), facilitating the collection of radiations from the film. To reduce background noises, a cold screen was placed behind the film. The screen was made of sheet copper, painted dull black, and cooled to 4 °C by a set of heat exchange coils welded to the back of the screen. To further improve the signal to noise ratio, the incoming IR signal was mechanically chopped at a frequency of 4000 Hz, preamplified, before sending to a lock-in amplifier (EG&G, Model 5209). Systematic methods were developed to calibrate the thermal radiometer and the procedures are detailed in Ref. 30.

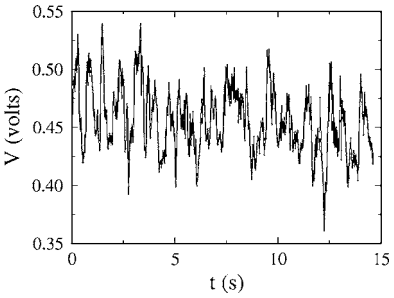

FIG. 4. A time trace of radiation signals from a soap film driven by a temperature gradient. The data were digitized at a rate of 1 kHz and at a 14-bit resolution. The measurement condition corresponds to $\Delta T = 55$ °C and $T_2 = 15.5$ °C. The large voltage fluctuations are due to passages of thermal plumes through the detection area (~1 mm in diameter) in the center of the film. The small-scale fluctuations are presumably due to fine internal structures of the plumes.

III. EXPERIMENTAL RESULTS

A. Temporal fluctuations of thermal radiation in thin films

We then proceeded to measure thermal radiation from the freely suspended soap film. Because a "stationary" film stratifies too rapidly that makes systematic measurements difficult, all of our experiments in the film were conducted in the presence of a temperature gradient. Figure 4 is a time trace of a typical run when $\Delta T = 41$ °C. One observes that radiation power fluctuates rapidly on different time scales from tens of milliseconds to ~1 s. The slow time scale is consistent with the visually observed rising and falling time of plumes. The fluctuation amplitude is ~100 mV that is significantly larger than the noise level of the lock-in output, which is less than 5 mV in the relevant frequency range of $0.1 < f < 1000$ Hz. The fluctuations have no discernible structures, suggesting that the flow is spatiotemporally chaotic or turbulent.

The time trace such as this one can be used to compute the power spectrum $\Gamma(f)$ of the radiated thermal power from the film. Figure 5 displays a set of three measurements carried out at three different vertical locations in the center region of the cell. As can be seen, the power spectrum $\Gamma(f)$ consists of two different regimes and is not very sensitive to the location where $\Gamma(f)$ is measured. For small frequencies, the spectrum displays a power-law-like behavior and can be mimicked by the function $\Gamma(f) \sim f^{-1.4 \pm 0.1}$ over a limited (about a half decade) frequency range. For large frequencies, the spectrum decays more rapidly and can be characterized by a different power law with $\Gamma(f) \sim f^{-4.2 \pm 0.8}$. The solid lines in the figures are guides to the eye. To ascertain that the fluctuations measured by the detector were indeed arising from the film, the measurement was repeated using the identical setting except the film was raptured. As shown by the lower curve in Fig. 5, even in the absence of the film the background radiation still contributes to the signal, but the magnitude is smaller by nearly three orders of magnitude in the low frequency part of the spectrum. This residual signal is due to the saturated water vapor above the soap solution

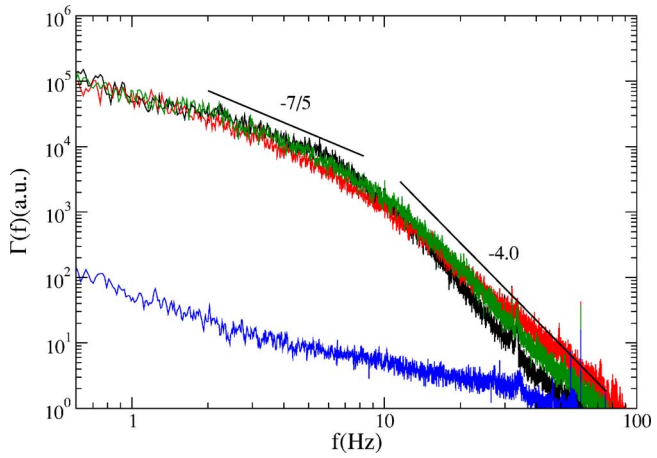

FIG. 5. The power spectra $\Gamma(f)$ of thermal radiation from a turbulent soap film. The upper curves were measured at the heights $y=1.3$ (black), 1.0 (green), and 0.7 cm (red), respectively, and the lower curve is the background without the film. The power spectra show two scaling regimes separated by a characteristic frequency $f_C \sim 7$ Hz. The scaling behavior $\Gamma(f) \sim f^{-1.4}$ in the low-frequency regime ($f < f_C$) is close to Bolgiano's theoretical prediction. See text for more details.

reservoir in the convection cell. The smallness of this background signal is reassuring, demonstrating the sensitivity of our measurement.

We also explored whether different confining geometries can affect the power spectrum. In 3D convection experiments, it was found that heat transport can be noticeably influenced by the topographic features of heated (or cooled) surfaces[40] and by the shape of the container.[41] However, it is unclear if the power spectrum itself were affected. In our 2D experiment, the geometric shape of confining cells are readily engineered as demonstrated in Fig. 6, where typical convection patterns in cells with a "rough" lower boundary (a), a semielliptical boundary (b), and a triangular boundary (c) are displayed. All these cells have an aspect ratio of unity and are made by milling of a thin stainless steel sheet. As can be seen in the figure (d), the measured $\Gamma(f)$ for three different cells yield essentially the same result for low frequencies, $\Gamma(f) \sim f^{-1.4}$, which is also seen in the square cell. The scaling behavior for high frequencies, however, is more varied with the exponent changing from 3.0 for the triangular cell to 4.4 for the semicircular cell. The similar spectral functions for different sample geometries are expected if the primary heat conduction is through the vapor phase rather than through the film.

The above observation suggests that for small frequencies or large spatial scales, there is a range of scales where the radiation power spectra exhibit self-similarity and appear to be universal independent of film shapes and the locations of the measurement. The spectrum $\Gamma(f) \sim f^{-1.4}$ is suggestive of a Bolgiano scaling,[29] but this measurement alone is insufficient to judge whether such a scaling arises because of temperature or density fluctuations. This question will be answered in the following subsection.

B. Spatial fluctuations of the film thickness determined by 2D IR imaging

In the above experiments, only the radiation power from the film has been measured. However, it is unclear the source of such fluctuations. Recall that the generalized Stefan-Boltzmann relation for a soap film is proportional to the product of s and T^4, where s is a function of the thickness h via Eq. (11). In order to address this issue, we resorted to direct thickness measurements using an IR camera (Inframet-

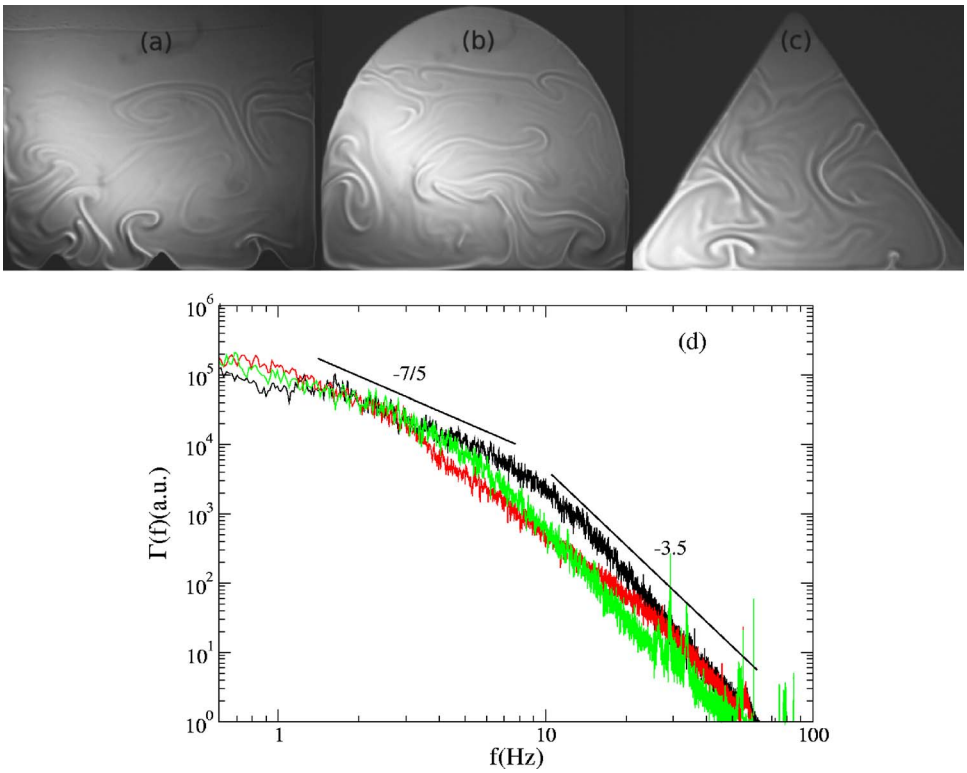

FIG. 6. The power spectra measured with different cell geometries. (a) A "rough" lower boundary, (b) a semielliptical boundary, and (c) a triangular boundary. The temperature difference was fixed at $\Delta T=41$ °C. Though thermal plumes are more likely to be emitted from the "rough" boundary, the measured power spectra, for the rough cell (green), the semielliptical cell (black), and the triangular cell (red), are approximately the same for low frequencies as displayed in (d).

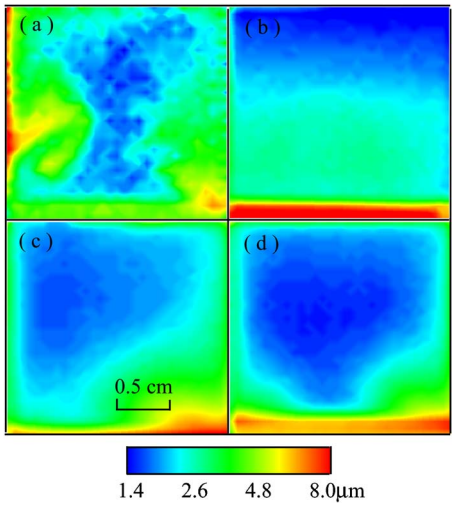

FIG. 7. Two-dimensional thickness maps measured by IR transmission. (a) This thickness map is calculated based on the snapshot of the IR transmission image taken at $\Delta T=61.5\ ^{\circ}\mathrm{C}$. The presence of a large-scale circulation, in this case clockwise, makes the thermal plumes to be generated near the side boundary of the cell. One can also observe small granular structures in the background, suggesting that the film thickness undulates on those scales. [(b)–(d)] These are ensemble averaged thickness maps obtained at $\Delta T=37\ ^{\circ}\mathrm{C}$ (b), $49.5\ ^{\circ}\mathrm{C}$ (c), and $61.5\ ^{\circ}\mathrm{C}$ (d), respectively. For the low temperature difference $\Delta T=37\ ^{\circ}\mathrm{C}$ (b), thermal plumes are predominantly generated from the bottom of the convection cell. As a result, the thickness stratifies uniformly in the vertical direction. For the intermediate temperature difference $\Delta T\sim 49.5\ ^{\circ}\mathrm{C}$ (c), some thermal plumes gain sufficient energy to climb to the top of the film. The convection takes place throughout the entire cell. However, the flow is a peculiar one in that the emission of thermal plumes is not symmetric along the horizontal direction. As the picture (c) shows, plumes are generated mostly from the lower right corner of the cell, breaking the left-right symmetry of the system. For a large temperature difference $\Delta T=61.5\ ^{\circ}\mathrm{C}$ (d), the large-scale circulation causes the film to be thick near the boundary and thin in the center. The left-right symmetry is largely recovered.

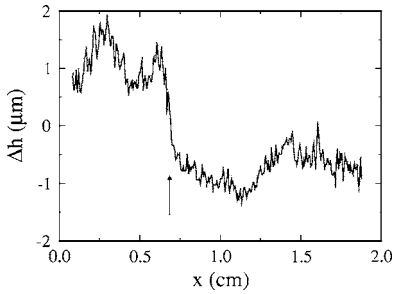

FIG. 8. Instantaneous thickness variations Δh along a center horizontal line of a turbulent soap film. This curve represents the thickness distribution along the vertical height, $y=1.2$ cm, of the film shown in Fig. 7(a). The mean thickness was subtracted. One observes that the thickness varies on large and small scales. Thermal plumes give the most significant contributions to the thickness variations. A sharp cliff, indicated by the arrow, can also be observed in the figure.

rics, Model 600 L). The camera uses the same light-sensing element (HgCdTe) as our homebuilt radiometer, and thus has the same spectrum range in the IR regime. To form an image, the camera's internal mirror scans line-by-line, forming images at a rate of 30 fps. The image consists of H256 $\times$V200 equivalent pixels and has an 8-bit resolution. Because water absorbs IR strongly, a transmission geometry is adopted in the measurement where the Lambert-Bear law can be used to find $h(=Z_0\ln(I_0/I)$.[27] Here I/I_0 is the normalized transmittance and Z_0 is the effective absorption length. For the given spectral width of the camera, our calculation shows that $Z_0=7.83\ \mu$m.[30]

In the transmission measurement, the cold screen was now replaced by a small hot plate (see Fig. 1), which was uniformly heated to $350\ ^{\circ}\mathrm{C}$. Since the plate was 20 cm away from the film, it had little effect on the film. The IR camera replaced the single-point detector and the transmission intensity from the film could be measured. In the absence of the film, the camera's sensitivity was adjusted such that each pixel was nearly saturated. Because the plate was a good radiator with $\varepsilon\sim 1$ and sufficiently hot compared to the film, in the absence of the plate, the pixel readings are uniformly zero for the given sensitivity setting. The gray scale of each pixel $I(x,y)$ normalized by its corresponding reading without the film $I_0(x,y)$ thus yields the transmittance of the film $t(x,y)=I(x,y)/I_0(x,y)$ at each point. A set of measurements at three different temperature differences, $\Delta T=37$, 49.5, and $61.5\ ^{\circ}\mathrm{C}$, were carried out. For each ΔT, 1000 images were collected at a time interval of 2 fps with the exposure time of 33 ms. The large time interval between the pictures ensures that thermal images are statistically independent, allowing ensemble averages of the mean thickness $\langle h(x,y)\rangle$ and its standard deviation $\langle \delta h(x,y)^2\rangle^{1/2}$ to be calculated.

Figure 7(a) is a typical snapshot of a thickness map converted from the transmission image according to the formula $h(x,y)=Z_0\ln(I_0(x,y)/I(x,y))$. Because the picture was taken at a relatively large temperature difference, $\Delta T=61.5\ ^{\circ}\mathrm{C}$, a LSC was present. In the picture, one clearly observes that a hot plume ejects near the sidewall instead of from the lower boundary, suggesting that the circulation is clockwise. The instantaneous thickness of the plume, $h\sim 5\ \mu$m, is considerably larger than the background thickness of $\sim 3\ \mu$m. As can also be seen from this instantaneous thickness map, the background h is not uniform, consisting of many granular structures. This suggests that h undulates on small scales, indicating turbulent velocity fluctuations are still active on those scales. Figure 8 is a horizontal cut along $y=1.2$ cm. The mean thickness has been subtracted from this measurement, and the data therefore represents the thickness variations δh along the horizontal line. Here the fine structures can be seen more clearly, and the interface between the plume and the background shows a sharp drop (or a cliff) as commonly seen in scalar turbulence with a large Schmidt number.[42]

A sequence of pictures such as Fig. 7(a) can be averaged, and the results are presented in Figs. 7(b)–7(d). For the low temperature difference $\Delta T=37\ ^{\circ}\mathrm{C}$, the average film thickness is uniformly stratified, thick near the bottom and thin at the top as evident in Fig. 7(b). There are very little variations in h along the horizontal direction, as one would expect by the symmetry of the system. Direct visual observations showed that at this low ΔT, thermal plumes are predominantly ejected from the bottom and they are not energetic enough to reach to the top of the film. The upper portion of the film therefore is relatively quiescent with only occasional incursions by a few powerful plumes. However, the lower

mixing region is a different case. Here thermal plumes carry fluid mass and kinetic energy, and efficiently stir up this part of film, making the thickness in this region not only more uniform but also thicker than the average. When ΔT increases, the plumes become more energetic and are able to ascend to a greater height in the film. As a consequence, the lower mixing zone expands with ΔT. Interestingly, by further increasing ΔT, when a significant number of hot plumes is able to reach to the top of the film, the dynamics of the system changes significantly; the film appears to lose its global balance in the sense that it tends to turnover, forming a LSC. However, near the threshold of the instability, it lacks the energy to sustain the circulation on such a large scale and the motion is rather intermittent and chaotic. Another interesting feature near the onset is that thermal plumes tend to accumulate at one of the lower corners of the convection cell, forming jets near that part of the side boundary. The system is very susceptible to perturbations or small imperfections in the setup, and the left-right symmetry of the system can be easily broken. For instance, it was observed that a tiny air bubble trapped near one corner of the cell was sufficient to bias the flow, causing plumes and jets to eject near that side of the convection cell. Figure 7(c) shows the flow near the threshold ($\Delta T_C = 48\ ^\circ\mathrm{C}$), where plumes are predominantly generated near the right boundary. Unlike the low ΔT case presented in Fig. 7(b), here the thickness profile shows variations both in the horizontal and the vertical directions.

When a sufficiently large $\Delta T (> \Delta T_C)$ was imposed on the film, LSCs were created in the cell. The flow chaotically switches the circulation directions from the clockwise to the counterclockwise and vice versa, and the left-right symmetry is partially restored. The LSC in thermal convection cell was first reported by Krishnamurti and Howard[43] and has been subsequently observed in many 3D experiments.[33,41,44–46] However, the physics behind this fascinating phenomenon still remains to be explained. Unlike 3D convection experiments, the period of persistent circulation in the film is much shorter, about a few seconds, instead of minutes.[45,47] Figure 7(d) shows the average thickness profile at $\Delta T = 61.5\ ^\circ\mathrm{C}$. The thickness distribution is very different from those observed when ΔT is small; h appears to be quite uniform near the center and the most thickness gradient appears near the boundary of the film, which is a result of the LSC.

To quantify our measurements, in Fig. 9 the mean thickness profile $h(y)$ (squares) and its standard deviation $\delta h(y)$ (circles) along the central vertical axis of the film are presented. Data are plotted for two temperature differences $\Delta T = 37\ ^\circ\mathrm{C}$ and $\Delta T = 61.5\ ^\circ\mathrm{C}$, corresponding to (b) and (d) of Fig. 7. In both cases, one observes that near the foot of the film ($y \sim 0$) the thickness is very large with h/Z_0 close to unity. However h decreases rapidly over a vertical height of a few millimeters. For the small temperature gradient $\Delta T = 37\ ^\circ\mathrm{C}$, the stratification above the foot is stable ($dh/dy < 0$), i.e., the 2D density decreases with y as shown by the solid line in (a). On the other hand, for the large temperature gradient $\Delta T = 61.5\ ^\circ\mathrm{C}$, the stratification above the foot is unstable ($dh/dy > 0$) with a small but discernible inverted thickness gradient as delineated in (b). We also noticed that overall the film thickness in the middle of the convection cell decreases as ΔT increases. Thus the onset of the LSC has the remarkable effect of not only homogenizing the mass distribution in the mixing zone along the vertical direction but also redistributing the mass as such that the density profile switches from the stable to the unstable configurations. Quantitatively, we found that h/Z_0 is about 20%–40% and $\delta h/Z_0$ is about 10% in different temperature gradients; the variance of the thickness $\delta h/Z_0$ is only weakly dependent on ΔT as shown by the circles in Figs. 9(a) and 9(b). For $Z_0 = 7.83\ \mu\mathrm{m}$, the average film thickness in the flowing soap film is $h \sim 2.2\ \mu\mathrm{m}$ and $\delta h \sim 0.8\ \mu\mathrm{m}$. It is reassuring that this measured h is in reasonably good agreement with that determined by the single-point radiometry measurement, where the averaged thickness was found to be $h \approx 1.7\ \mu\mathrm{m}$. The small ratio h/Z_0 causes the thermal emissivity of the film to fluctuate and is the dominant source of temporal fluctuations in the detected radiation signal.

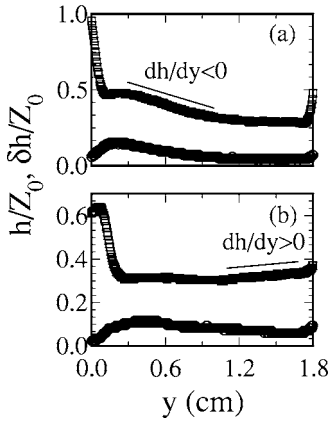

FIG. 9. The vertical mean thickness profile $h(y)$ and the standard deviation $\delta h(y)$. Both measurements (a) and (b) were made along the central vertical axis of the film using the thickness maps presented in Figs. 7(b) and 7(d). The top figure (a) corresponds to $\Delta T = 37\ ^\circ\mathrm{C}$ and the bottom figure (b) corresponds to $\Delta T = 61.5\ ^\circ\mathrm{C}$. In both cases, the average film thickness h is represented by the squares and the standard deviation δh is represented by circles. The horizontal axis is the vertical height y of the film.

C. Statistics and scaling relations for 2D density fluctuations

Returning to the single-point measurement, the physics underlying the power spectra observed in Figs. 5 and 6(d) now become clear. What we have observed is essentially the 2D density fluctuations of the film. It has been postulated in the 50 s by Bolgiano that convective turbulence in a stably stratified fluid, such as in the earth atmosphere or in oceans where air or salt molecules can form stable density gradients, shall behave very differently from Navier-Stokes turbulence in a homogeneous medium.[29] The difference stems from the fact that there is constant "tradeoff" of the kinetic energy and the gravitational potential energy such that the energy flux ε on large scales is no longer a constant but depends on the measurement length scale l. The situation is in contrast with turbulence in a fluid with a uniform density, where ε general does not depend on l in the inertial range and the Kolmogorov 5/3-law follows.[48]

It is possible to generalize Bolgiano's scaling argument to convection in soap films. In accordance with such a theory, we assumed that the time rate of change of 2D density fluctuations ($\delta\rho_2=\rho\delta h$) is a constant of motion $\chi_\rho=d\langle\delta\rho_2^2\rangle/dt=$const such that

$$\langle\delta\rho_{2l}^2\rangle \sim \chi_\rho l/v_l, \tag{12}$$

where ρ_{2l} and v_l are, respectively, the 2D density and velocity on scales l. Assuming that potential energy and the kinetic energy are balanced on the scale l ($\rho_2 v_l^2/2=\delta\rho_2 gl$), which is true only for large scales, one finds $v_l\sim(2gl(\delta\rho_{2l}/\rho_2))^{1/2}$. Replacing v_l in Eq. (12), one arrives at the scaling relation for the structural function for $\delta\rho_{2l}$,

$$\langle\delta\rho_{2l}^2\rangle \sim \chi_\rho^{4/5}(g/\rho_2)^{-2/5}l^{2/5}. \tag{13}$$

In the momentum space, the corresponding relationship is the power spectrum that scales as $\Gamma(k)\sim k^{-7/5}$,[29] where $k=2\pi/l$ is the wave number. Thus, the power spectrum for density fluctuations on large spatial scales is expected to be identical in 2D and 3D, despite the fact that energy flux in 2D is reversed as seen in our earlier experiment.[49] The predicted scaling for $\Gamma(k)$ is nearly identical to what we have observed $f^{-1.4\pm0.1}$ for different cell geometries presented in Figs. 5 and 6(b). The only difference is that the measurements were carried out in the frequency space whereas the calculation is for the momentum space. However, such a difference can be reconciled if one takes the view that small-scale fluctuations are convected by large-scale flows with the result $f=v_{\rm rms}/l$.[50] On a more fundamental level, the same scaling relation in the frequency domain (our measurements) and in the wave number domain (theory) may be expected and is a result of the extension of Kolmogorov's refined similarity hypothesis (K62) (Ref. 51) to the scalar field. The K62, originally formulated for the velocity field, postulates that if one measures the longitudinal velocity difference δv_l on the scale l and simultaneously measured (coarse-grained) energy dissipation rate ε_l on the same scale, one can form a new random valuable $V(1,0,0,0)=\delta v_l/(l\varepsilon_l)^{1/3}$ such that $P(V)$ is *only a function* of locally defined Reynolds numbers $\mathrm{Re}_l=l\delta v_l/\nu$, where the four indices of V stands for the longitudinal, the two transverse components of velocity, and the time. It was further conjectured that V and ε_l are statistically independent and for $\mathrm{Re}_l\gg1$,$P(V)$ becomes independent of Re_l and is a universal function. As we can see, although the K62 did not make any statement about the form of $P(V)$, it did not exclude the possibility of using the time difference δt for forming the random valuable $V(0,0,0,1)$ and the pdf would be universal independent of whether V is calculated based on distance or time. For the velocity field, K62 was reasonably well supported in fully developed 3D turbulence.[52] It seems plausible that the idea of K62 could be generalized to a scalar quantity and the statistical distribution of the quantity would be independent of whether it is measured in space or in time. However, to our knowledge, this idea has not been rigorously tested in laboratory experiments so far.

The two spectral ranges observed in the experiment allow us to define the crossover frequency f_C, which turns out to be ~7 Hz. Using the simple relation $l_C\sim v_{\rm rms}/f_C$ and the measured $v_{\rm rms}\sim3$ cm/s, the crossover length is ~0.4 cm. This length scale is comparable to the plume size in the middle of the cell and can also be compared to the Bolgiano's length scale $l_B\sim0.27$ cm calculated based on the parameters of our system.[49] Physically l_B is the scale where the gravitational energy and the kinetic energy are approximately balanced.[29]

While the $k^{-1.4}$ scaling for the low-frequency regime was found to be robust, the corresponding scaling relation for the high-frequency regime is less reliable. Variations from k^{-3} to $k^{-4.5}$ were observed in a range of temperature differences ($20<\Delta T<62\ ^\circ$C) and for different sample geometries. There have been intense debates on what should be the proper scaling laws for length scales $l(=2\pi/k)$ less than the Bolgiano length l_B but larger than the Kolmogorov energy dissipation scales l_D, $l_D<l<l_B$, namely, within the classical Kolmogorov's inertial range. Bolgiano's theoretical analysis suggests that for $l<l_B$, the density behaves like a passive scalar and has the spectrum $\Gamma(k)\sim k^{-5/3}$. Our measurement in the high-frequency regime clearly violates this scaling law. In a different derivation, Wheelon[53] and Villars and Wiskopf[54] assumed that density fluctuations are created by turbulent velocity itself, instead of "feeding" by the large-scale gradient, and found $\Gamma(k)\sim k^{-3}$. This scaling exponent is still smaller than but is closer to our measured value 3.7 ± 0.8. Based on the experimental observations, it is also possible that the high-frequency spectrum may be influenced by the plume structures as well as their emission statistics. In this case, new physics related to plumes, rather than the large-scale density gradient, are required in order to interpret our observations.

It is clear from the above measurements that strong density variations in space and time are the hallmark of convection in freely suspended soap films. The 2D density $\delta\rho_2$ is thus an active scalar that couples strongly to the velocity field. However, certain statistical properties of $\delta\rho_2$ were found to be remarkably similar to a passive scalar such as a dye in turbulent flows. For instance, we can use the time trace from the single-point detector, such as the one in Fig. 4, to construct the probability density function (pdf) for the density difference $\delta\rho_2(\tau)$, where τ is the temporal separation between two points. It is understood that the temporal separation is related to the spatial separation by $l\approx v_{\rm rms}\tau$. As delineated in Fig. 10(a), the $P(\delta\rho_2(\tau))$ exhibits two remarkably different behaviors depending on τ. For a small τ, the pdf has the typical triangular shape on this semilogarithmic plot, indicating that the wings of the pdf are exponential. On the other hand, for a large τ, the pdf is, to a good approximation, a Gaussian function. We also noticed that for $\tau>0.4$ s, all the pdfs become identical, indicating that the density fluctuations have reached an outer scale, which we determined to be $l_0\sim v_{\rm rms}\tau\sim1.2$ cm. The scale l_0 can be identified as the largest eddy in the flow and is about half the size of the soap film.

Another conspicuous feature of the pdfs is that they are skewed towards the positive side. The magnitude of the skewness $S_\tau=\langle\delta h(\tau)^3\rangle/\langle\delta h(\tau)^2\rangle^{3/2}$ is substantial and is dependent on τ or l. Figure 10(b) shows that S_τ is large in the

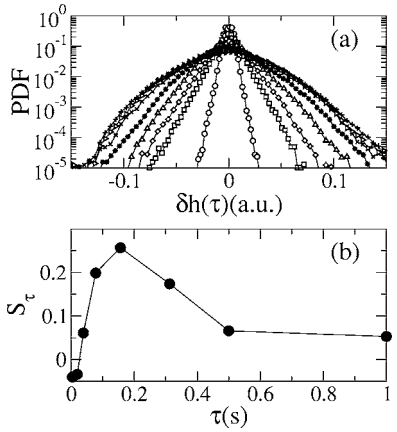

FIG. 10. Probability density functions $P(\delta\rho_2(\tau))$ of the film thickness variations vs time difference τ. (a) Different symbols correspond to $\tau=1/256$ (open circles), 5/256 (open squares), 10/256 (diamonds), 20/256 (triangles), 40/256 (asterisks), 80/256 (crosses), 0.5 (tilted triangles), and 1.0 s (pluses). (b) The skewness S_τ as a function of τ. We noted that the skewness is significantly greater in the range $0.1<\tau<0.5$ s, which corresponds to the Bolgiano regime.

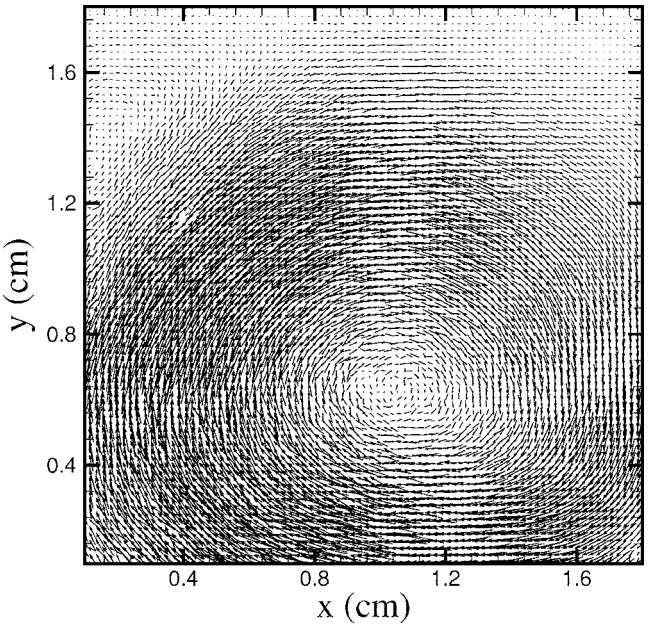

FIG. 11. The ensemble averaged mass flux in the presence of a large-scale circulation. Simultaneous velocity and thermal radiation fields were measured at $\Delta T=61.5\ ^\circ$C. This allows the local mass flux to be calculated. Even after averaging over 500 fields, the mass flux is still nonzero, showing a large-scaling loop in the clockwise direction. The loop is squashed vertically as a result of density stratification.

Bolgiano regime, $0.1<\tau<0.5$ s, and reaches a peak value of 0.25. We believe that this positive skewness is due to the plume structure, i.e., a plume has a compressed front with a large 2D density gradient and a gentler opposite gradient in the interior. This forms the so-called cliff-ramp structure and is the source of the skewness. Since the measurement was carried out in the center of the cell and in the presence of a LSC, the most frequent events are large falling plumes that pass through the detecting volume. The rarity of small rising plumes in the center of the cell also explains the small S_τ value for $\tau\rightarrow 0$ as shown in Fig. 10(b). The nonvanishing skewness has been observed for a passive scalar, such as temperature fluctuations in a wind tunnel, when a linear temperature gradient is imposed.[55] However, it is interesting to notice that as far as the skewness is concerned, an active scalar, such as the 2D density of the film, behaves similarly as a passive scalar, the temperature in the wind tunnel.

D. Full-field 2D density flux measurements

For turbulent studies, it is of fundamental interest to measure fluxes because they determine the rate of transport of various quantities from scale to scale. In the current case, the quantity of interest is the mass density flux $\mathbf{j}=\rho h(x,y)\mathbf{v}(x,y)$. We have performed simultaneous measurements of the thickness $h(x,y)$ and the velocity field $\mathbf{v}(x,y)$ using the IR camera and the PIV. In Sec. II C, it has been shown that within the spectral range of the camera, $8<\lambda<14$ μm, the thermal emissivity s is given by $s\approx h/Z_0$ when $h\ll Z_0$. Thus the IR camera yields an intensity map $I(x,y)$ that are related to thermal emission from the film according to the Stefan-Boltzmann law $s\sigma T^4$. Combining $I(x,y)$ with the velocity field $\mathbf{v}(x,y)$ acquired by the PIV, the following pseudo flux can be constructed, $\mathbf{J}(x,y)\sim(h/Z_0)\sigma T^4\mathbf{v}=(\sigma/Z_0)(\bar{h}+\delta h)(\bar{T}+\delta T)^4\mathbf{v}$, where $\bar{h}(y)$ and $\bar{T}(y)$ are the average film thickness and temperature, which are functions of y only. The linearized form of the above equation, taking into account $\delta h/\bar{h}\gg\delta T/\bar{T}$, is given by $\mathbf{J}(x,y)\sim\sigma/Z_0\bar{T}^4\bar{h}(1+\delta h/\bar{h})\mathbf{v}$. If a time average is performed, the density flux has a simple form given by $\mathbf{J}(x,y)\sim(\sigma/Z_0)\bar{T}^4\langle\delta h(x,y)\mathbf{v}(x,y)\rangle$, where we have used the fact that $\langle\mathbf{v}(x,y)\rangle=0$ in the steady state. As can be seen, $\bar{J}(x,y)$ and $\mathbf{j}(x,y)$ differ only by a numerical constant.

The thermal images acquired by the IR camera and the velocity fields acquired by the PIV were synchronized by a video acquisition board in a PC computer. For each point in the film, the local density flux was calculated by combining the two images. Although the individual flux maps appear to be uncorrelated from frame to frame, because of the rate of image acquisition was low (2 Hz), the time-averaged map shows interesting structures as delineated in Fig. 11. Specifically, we found that even after ~500 averages spanning several minutes of measurement time, the map displays a closed loop occupying the entire cell. Such a large coherent structure is surprising considering that the total time of averaging is much longer than the typical switching time of the LSC, which is about a second or so. This indicates that the system is biased, although such a bias is not discernible to the naked eye. We also noted that the center of the circulation does not coincide with the geometrical center of the convection cell despite $\Delta T(=62\ ^\circ\text{C})$ is significantly above $\Delta T_C(\approx 48\ ^\circ\text{C})$. The squeezing of the flux pattern in the vertical direction suggests that even in this kinetic-energy dominated regime, the gravitational potential energy still exerts its influence, making fluctuations in the horizontal and vertical direction different.

IV. SUMMARY

Using a homebuilt radiometer, we have successfully measured thermal radiation from a freely suspended soap film subject to a vertical temperature gradient. Since for the current experiment, the average film thickness is less than the absorption length of the IR radiation ($h/Z_0<1$), the temporal fluctuation of the radiation signal is dominated by the 2D density fluctuations via the thermal emissivity of the film. The average film thickness profiles are measured, and the strong mean density gradients are shown to be the cause of asymmetric emission of thermal plumes. We find for the first time that 2D mass density can switch from the stable to the unstable stratification as the temperature difference ΔT is increased, $\Delta T>\Delta T_C$. Our observation indicates that this transition is closely related to the elimination of the stably stratified top layer when thermal plumes gain sufficient energy in a large temperature gradient. In our 2D system, the inverted density profile then brings about a large-scale-circulation, which shares many common features of LSC in 3D Rayleigh-Bénard systems. However, it is not known if the same mechanism, i.e. the density inversion, occurs in 3D systems. Near the onset, the formation of the LSC in our system is found to be very sensitive to minute biases and local perturbations. Even with runs that appear to eliminate all imperfections, the long-time average of the density flux still exhibits large coherent structures as shown in Fig. 11.

We have also investigated temporal fluctuations of 2D mass density at a single point in the center of the film. The measured power spectra are in good agreement with the Bolgiano's theoretical calculation.[29] Specifically, in the low-frequency regime, the power spectrum exhibits the scaling $\Gamma(f)\sim f^{-1.4}$. In the high-frequency regime, on the other hand, $\Gamma(f)\sim f^{-\beta}$ with β being between 3 and 4.5. This latter behavior is inconsistent with Bolgiano's theory and is not well understood at this stage.

Finally, we would like to point out that the noninvasive technique implemented in the current study has a great potential for future research. Our analysis shows that it is feasible to measure temperature variations in the film if the detector is operated around the 3 μm wavelength range, where water molecules absorb electromagnetic waves most strongly with the extinction length Z_0 less than a micron. In this strong absorption regime, a film of a few microns in thickness is essentially opaque, behaving like an ideal blackbody with the thermal emissivity close to unity. In this case, the measured radiation power gives a direct measurement of the local temperature in the film. Thus by IR imaging with different wavelengths and particle tracking, all important quantities relevant to thermal convection in the soap film, such as $\rho_2(x,y)$, $T(x,y)$, and $\mathbf{v}(x,y)$, are accessible to experimenters. This would give much thrust in the study of convective turbulence in two dimensions.

ACKNOWLEDGMENTS

We would like to thank K.-Q. Xia for his early participation in this project. We are also grateful to Dr. F. Miller and Dr. J. Kizito at the NASA Glenn Research Center who generously allowed us to use their IR camera and to Y. Jun who provided technical assistance. This work is supported by NASA under Grant No. NAG3-2730 and by NSF under Grant No. DMR-0242284.

[1] Y. Couder, J. M. Chomaz, and M. Rabaud, "On the hydrodynamics of soap films," Physica D **37**, 384 (1989).
[2] M. Gharib and P. Derango, "A liquid film tunnel to study two dimensional laminar and turbulent shear flows," Physica D **37**, 406 (1989).
[3] H. Kellay, X. L. Wu, and W. I. Goldburg, "Experiments with turbulent soap films," Phys. Rev. Lett. **74**, 3975 (1995).
[4] J. M. Burgess, C. Bizon, W. D. McCormick, J. B. Swift, and H. L. Swinney, "Instability of the Kolmogorov flow in soap film," Phys. Rev. E **60**, 715 (1999).
[5] J. Zhang, S. Childress, A. Libchaber, and M. Shelley, "One-dimensional flags in a two-dimensional wind," Nature (London) **408**, 835 (2000).
[6] M. A. Rutgers, X. L. Wu, and W. B. Daniel, "Conducting fluid dynamics experiments with vertically falling soap films," Rev. Sci. Instrum. **72**, 3025 (2001).
[7] M. Rivera and X. L. Wu, "Homogeneity and the inertial range in driven 2D turbulence," Phys. Fluids **14**, 3098 (2002).
[8] P. C. Tsai, Z. Daya, and S. W. Morris, "Aspect-ratio dependence of charge transport in turbulent electroconvection," Phys. Rev. Lett. **92**, 084503 (2004).
[9] P. C. Tsai, Z. Daya, and S. W. Morris, "Charge transport scaling in turbulent electroconvection," Phys. Rev. E **72**, 046311 (2005).
[10] J. M. Chomaz, "The dynamics of a viscous soap film with soluble surfactant," J. Fluid Mech. **442**, 387 (2001).
[11] R. H. Kraichnan and D. Montgomery, "Two-dimensional turbulence," Rep. Prog. Phys. **43**, 547 (1980).
[12] M. Chertkov, G. Falkovich, I. Kolokolov, and V. Lebedev, "Statistics of a passive scalar advected by a large-scale two-dimensional velocity field," Phys. Rev. E **51**, 5609 (1995).
[13] A. Bracco, J. C. McWilliams, G. Murante, A. Provenzale, and J. B. Weiss, "Revisiting freely decaying two-dimensional turbulence at millennial resolution," Phys. Fluids **12**, 2931 (2000).
[14] C. I. Christov and G. M. Homsy, "Nonlinear dynamics of two-dimensional convection in a vertically stratified slot with and without gravity modulation," J. Fluid Mech. **430**, 335 (2001).
[15] B. Martin and X. L. Wu, "Double-diffusive convection in freely suspended soap films," Phys. Rev. Lett. **80**, 1892 (1998).
[16] M. I. Godfrey and D. H. Van Winkle, "Surface-tension-gradient-induced flow in freely suspended liquid crystal films," Phys. Rev. E **54**, 3752 (1996).
[17] J. Birnstock and R. Stannarius, "Vertically suspended smectic films with in-plane temperature gradients," Mol. Cryst. Liq. Cryst. Sci. Technol., Sect. A **366**, 815 (2001).
[18] D. R. Moore and N. O. Weiss, "Two-dimensional Rayleigh-Benard convection," J. Fluid Mech. **58**, 289 (1973).
[19] J. H. Curry, J. R. Herring, J. Loncaric, and S. A. Orszag, "Order and disorder in two- and three- dimensional Benard convection," J. Fluid Mech. **147**, 1 (1984).
[20] J. Werne, "Structure of hard-turbulent convection in two dimensions: Numerical evidence," Phys. Rev. E **48**, 1020 (1993).
[21] A. Celani, A. Mazzino, and M. Vergassola, "Thermal plume turbulence," Phys. Fluids **13**, 2133 (2001).
[22] D. Biskamp, K. Hallatschek, and E. Schwarz, "Scaling laws in two-dimensional turbulent convection," Phys. Rev. E **63**, 045302 (2001).
[23] T. M. Rogers, G. A. Glatzmaier, and S. E. Woosley, "Simulation of two-dimensional turbulent convection in a density-stratified fluid," Phys. Rev. E **67**, 026315 (2003).
[24] C. Bizon, J. Werne, A. A. Predtechensky, K. Julien, W. D. McCormick, J. B. Swift, and H. L. Swinney, "Plume dynamics in quasi-2D turbulent convection," Chaos **7**, 107 (1997).
[25] M. Assenheimer and V. Steinberg, "Rayleigh-Bénard convection near the gas-liquid critical point," Phys. Rev. Lett. **70**, 3888 (1993).
[26] J. Zhang, X. L. Wu, and K. Q. Xia, "Density fluctuations in strongly stratified two-dimensional turbulence," Phys. Rev. Lett. **94**, 174503 (2005).
[27] X. L. Wu, R. Levine, A. Belmonte, and W. I. Goldburg, "Infrared technique for measuring thickness of a flowing soap film," Rev. Sci. Instrum. **72**, 2467 (2001).
[28] H. Kellay, "Dispersion in the enstrophy cascade of two-dimensional decaying turbulence," Phys. Rev. E **69**, 036305 (2004).

[29]R. Bolgiano, Jr., "Turbulent spectra in a stably stratified atmosphere," J. Geophys. Res. **64**, 2226 (1959).
[30]J. Zhang, "Thermal convection in vertically suspended soap films," Ph.D. thesis, University of Pittsburgh (2005).
[31]W. Merzkirch, *Flow Visualization* (Academic, New York, 1987).
[32]F. H. Busse, "Nonlinear properties of thermal convection," Rep. Prog. Phys. **41**, 1929 (1978).
[33]B. Castaing, G. Gunaratne, F. Heslot, L. Kadanoff, A. Libchaber, S. Thomae, X.-Z. Wu, S. Zaleski, and G. Zanetti, "Scaling of hard thermal turbulence in Rayleigh-Benard convection," J. Fluid Mech. **204**, 1 (1989).
[34]J. A. Glazier, T. Segawa, A. Naert, and M. Sano, "Evidence against 'ultrahard' thermal turbulence at very high Rayleigh numbers," Nature (London) **398**, 307 (1999).
[35]J. J. Niemela, L. Skrbek, K. R. Sreenivasan, and R. J. Donnelly, "Turbulent convection at very high Rayleigh numbers," Nature (London) **404**, 837 (2000).
[36]X. L. Qiu and P. Tong, "Large-scale velocity structures in turbulent thermal convection," Phys. Rev. E **64**, 036304-1 (2001).
[37]For air being an ideal conductor, γ' can be calculated explicitly with the result $\gamma' = \kappa(\rho^2/\rho_2)^2$. However, this is a drastic assumption, which significantly overestimates the heat loss in the film. In future experiments, γ' may be measured directly in partial vacuum similar to the experiment of Ref. 38.
[38]B. K. Martin, X. L. Wu, W. I. Goldburg, and M. A. Rutgers, "Spectra of decaying turbulence in a soap film," Phys. Rev. Lett. **80**, 3964 (1998).
[39]X. L. Ma, C. C. Moeller, W. P. Menzel, and L. E. Gumley, "Simultaneous retrieval of atmospheric profiles, land-surface temperature, and surface emissivity from moderate resolution imaging spectroradiometer thermal infrared data: extension of a two-step physical algorithm," Appl. Opt. **41**, 909 (2002).
[40]Y. Shen, P. Tong, and K.-Q. Xia, "Turbulent convection over rough surfaces," Phys. Rev. Lett. **76**, 908 (1996).
[41]Z. A. Daya and R. E. Ecke, "Does turbulent convection feel the shape of the container?" Phys. Rev. Lett. **87**, 184501 (2001).
[42]M. Holzer and E. D. Siggia, "Turbulent mixing of a passive scalar," Phys. Fluids **6**, 1820 (1994).
[43]R. Krishnamurti and L. N. Howard, "Large-scale flow generation in turbulent convection," Proc. Natl. Acad. Sci. U.S.A. **78**, 1981 (1981).
[44]X. Z. Wu and A. Libchaber, "Scaling relations in thermal turbulence: The aspect-ratio dependence," Phys. Rev. A **45**, 842 (1992).
[45]X.-L. Qiu and P. Tong, "Temperature oscillations in turbulent Rayleigh-Benard convection," Phys. Rev. E **66**, 026308 (2002).
[46]X.-D. Shang, X.-L. Qiu, P. Tong, and K.-Q. Xia, "Measured local heat transport in turbulent Rayleigh-Benard convection," Phys. Rev. Lett. **90**, 074501 (2003).
[47]M. Sano, X. Z. Wu, and A. Libchaber, "Turbulence in helium-gas free convection," Phys. Rev. A **40**, 6421 (1989).
[48]A. N. Kolmogorov, "The local structure of turbulence in incompressible viscous fluid for very large Reynolds number," Dokl. Akad. Nauk SSSR **30**, 9 (1941).
[49]J. Zhang and X. L. Wu, "Velocity intermittency in a buoyancy subrange in a two-dimensional soap film convection experiment," Phys. Rev. Lett. **94**, 234501 (2005).
[50]V. S. L'vov, "Spectra of velocity and temperature fluctuations with constant entropy flux of fully developed free-convective turbulence," Phys. Rev. Lett. **67**, 687 (1991).
[51]A. N. Kolmogorov, "A refinement of previous hypotheses concerning the local structure of turbulence in a viscous incompressible fluid at high Reynolds number," J. Fluid Mech. **13**, 82 (1962).
[52]G. Stolovitzky, P. Kailasnath, and K. R. Sreenivasan, "Kolmogorov's refined similarity hypothesis," Phys. Rev. Lett. **69**, 1178 (1992).
[53]A. D. Wheelon, "Spectrum of turbulent fluctuations produced by convective mixing of gradients," Phys. Rev. **105**, 1706 (1957).
[54]F. Villars and V. F. Weisskopf, "The scattering of electromagnetic waves by turbulent atmospheric fluctuations," Phys. Rev. **94**, 232 (1954).
[55]L. Mydlarski and Z. Warhaft, "Passive scalar statistics in high-Peclet-number grid turbulence," J. Fluid Mech. **358**, 135 (1998).